Contents lists available at ScienceDirect

Transactions of Nonferrous Metals Society of China

36(2026) 371−385

www.tnmsc.cn

Microstructure evolution mechanism during creep aging and creep response of Al−Zn−Mg−Cu alloys under different aging treatments

Chuan GAO [a], Xiao-bin GUO [b], Feng-quan WANG [a], Chao-jie LIANG [b], Yun-lai DENG [a,b,*]

[a] Light Alloy Research Institute, Central South University, Changsha 410083, China;

[b] School of Materials Science and Engineering, Central South University, Changsha 410083, China

Abstract: The creep response, mechanical properties, and microstructure evolution of the Al−Zn−Mg−Cu alloy were investigated under different initial heat treatment conditions. The results indicate that the density of geometrically necessary dislocations (GNDs) increases during the initial creep stage (<0.5 h) and undergoes dynamic changes in the stable creep stage. During creep aging, the dislocation distribution within the grains becomes more uniform, and additional subgrains are formed. The key factors influencing creep behavior are crystal orientation and the degree of initial precipitation. Grains oriented in the ⟨001⟩ and ⟨101⟩ directions are more susceptible to deformation during the creep process. Based on a strength model, the inhibitory effects of the η' phase in T6 specimens and the GP I zone in T4 specimens on dislocation motion were evaluated. This study demonstrates that selecting an appropriate initial precipitation state is an effective strategy to enhance the creep aging response and to produce high-performance components.

Keywords: Al−Zn−Mg−Cu alloy; creep aging; quasi-in-situ EBSD; microstructure; crystal orientation; initial precipitation state

1 Introduction

The Al−Zn−Mg−Cu alloy exhibits excellent properties, including low density, high strength, and high fatigue resistance, making it widely used in the manufacture of large aircraft skins, wall panels, and other structural components [1−3]. Specifically, the mechanical properties of heat-treatable Al−Zn−Mg−Cu alloys are primarily determined by the aging precipitated phase [4−6] and dislocation density [7,8], with the type, size and distribution of the precipitated phases dominant [9,10]. However, fracture and springback are likely to occur in the forming of complex structural components due to the alloy's poor formability. As a solution, creep aging has been introduced as a leading technology [11]. Moreover, creep-formed components exhibit lower residual stresses, which enhances their resistance to both fatigue and stress corrosion cracking, ultimately improving service performance [12].

The manufacturing process of thin-walled parts typically involves plastic forming followed by creep aging. Most of the component's deformation is completed during the plastic forming stage, and it is widely recognized that plastic deformation leads to significant stress concentration [13,14]. In the process of creep aging, stress relaxation and artificial aging are completed to obtain the final product size and final mechanical properties. Recently, numerous studies have investigated the effects of heat treatment methods during creep age forming (CAF) on the creep deformation and properties of aluminum alloys. The creep formability and properties after creep are improved through various methods, including pre-aging, combined treatment of

Corresponding author: *Yun-lai DENG, Tel: +86-13873152095, E-mail: 131258@csu.edu.cn

https://doi.org/10.1016/S1003-6326(25)66970-6

Received 27 May 2024; accepted 8 January 2025

pre-aging and pre-deformation, electropulsing assistance and multistage creep aging [15−18]. MAHATHANINWONG et al [19] demonstrated that T6 heat treatment of 7075 aluminum alloy can reduce creep formability due to the high density of dispersed precipitates, which effectively hinders dislocation movement. LIN et al [16] found that the corrosion resistance and creep formability can be effectively improved after retrogression and re-aging (RRA) and pre-stretching treatment.

It is widely recognized that the dislocation caused by strain can influence both the microstructure and mechanical properties [20−22]. LU et al [23] investigated the dislocation density changes before and after creep aging in Al−Zn−Mg−Cu alloys using X-ray diffraction (XRD). WANG et al [24] analyzed the dislocation density evolution of Al−Li alloy under different stress levels using XRD. However, in these studies, the potential error introduced by specimen replacement was not considered, making it challenging to observe the evolution of dislocation movement. Therefore, in this study, a quasi-in-situ electron backscattered diffraction (EBSD) research method was used to track the evolution of GNDs during the creep aging process.

In the present work, we designed two kinds of heat treatment states of the Al−Zn−Mg−Cu alloy, and studied the influence of the initial degree of precipitation and crystal orientation on creep behavior and the microstructural evolution. The orientation dependence of creep age forming was studied by quasi-in-situ EBSD. Combined with transmission electron microscopy (TEM) analysis, the movement resistance of dislocation under different precipitation conditions was estimated.

2 Experimental

2.1 Material preparation

The material used in this study was an Al−Zn−Mg−Cu alloy with a chemical composition of Al−7.5Zn−1.5Mg−1.4Cu−0.15Zr (wt.%), in the hot-rolled condition with a thickness of 4 mm. The composition of this alloy closely resembles that of commercial aluminum alloy 7085. The tensile and creep tensile specimens, with dimensions as shown in Fig. 1**,** were cut along the rolling direction of the Al−Zn−Mg−Cu alloy sheet. Figure 2 illustrates the material preparation and creep testing processes. Specimens of two different initial heat treatment states, namely natural aging state and peak aging state, were prepared before creep aging. The specific preparation procedures were as follows.

(1) Natural aging (T4) specimen preparation: Solid-solution treatment was carried out at 470 °C for 1 h. The specimen was immediately taken out after room temperature water quenching, and transfer time should not exceed 5 s. The specimens were subjected to natural aging at room temperature, and the aging time was 168 h.

(2) Peak aging (T6) specimen preparation: Solid-solution treatment was carried out at 470 °C for 1 h. The specimen was immediately taken out after room temperature water quenching, and transfer time should not exceed 5 s. The specimens were kept in an aging furnace at 120 °C for 24 h, and then immediately quenched in water at room temperature.

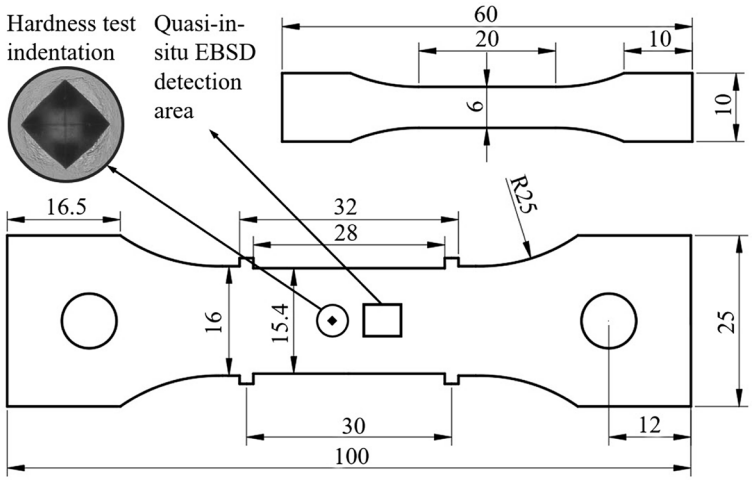

Fig. 1 Dimensions of tensile and creep tensile specimens of Al−Zn−Mg−Cu alloy and quasi-in-situ EBSD detection area (Unit: mm)

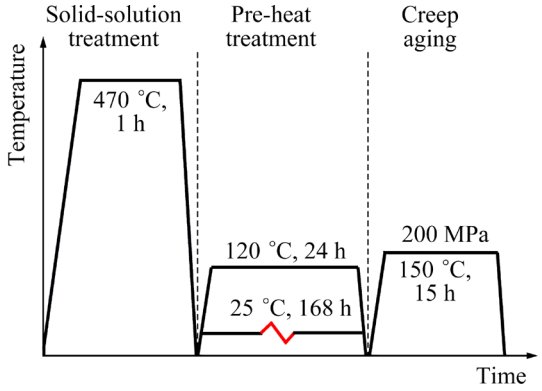

Fig. 2 Experimental schedule of Al−Zn−Mg−Cu alloy

2.2 Mechanical properties tests

For Al−Zn−Mg−Cu alloys, creep aging experiments are generally performed at 120−200 °C in order to regulate the aging response rate. The constant stress creep relaxation test temperature is 150 °C, which is suitable for 7xxx series aluminum alloy [25−27].

The uniaxial tensile test was performed using the RWS 50 electronic creep relaxation testing machine. A tensile stress of 200 MPa was applied along the axis of the specimen, and the loading rate for all samples was 15 N/s. The creep aging temperature was 150 °C and the heating time was less than 10 min, so the effect of aging treatment on the material properties can be neglected. To ensure that the sample reached the desired temperature quickly, the clamping device of the creep relaxation machine was preheated to 150 °C, and the temperature was monitored and controlled via thermocouples positioned at the upper, middle, and lower sections of the specimen. During the creep aging process, the tensile stress should not exceed the yield limit of the material, in order to achieve optimal strengthening. The yield strengths of the T4 and T6 specimens were tested to be (310.0±5.0) and (495.5±5.5) MPa, respectively. In order to prevent the specimens from breaking during the creep aging process, the creep test condition was 200 MPa and 15 h. After the creep aging process, the specimens were air-cooled to room temperature.

2.3 Microstructure characterization

Figure 3 illustrates the schematic diagrams of a quasi in-situ EBSD test, using the EVO MA10 SEM with the Oxford EBSD detector. Specimen preparation consisted of grinding, polishing, and anodizing of the freshly polished surface in a cooled and stirred electrolyte for 7 s. The voltage was 20 V and the electrolyte was 30% $HClO_4$ + 70% C_2H_5OH (volume fraction). Huayin SHYCHVT−5 Z-type Vickers hardness tester was used to press the specimen with a test force of 29.3 N and a retention time of 15 s. The hardness test indentation was used as anchor points for quasi-in-situ EBSD characteristics in the nearby area. The same specimen was observed with EBSD when the creep aging treatment time was 5, 10 and 15 h, respectively, and at least three areas were scanned for each specimen. The EBSD scan step size was set as 1.2 μm.

Low-angle grain boundaries (LAGBs) with a difference of orientation between 2° and 15° are depicted as yellow lines, and high-angle grain boundaries (HAGBs) with a difference of orientation greater than 15° are depicted as black lines. The EBSD data were analyzed by the Channel 5 analysis software, and the kernel average misorientation (KAM) was analyzed by the TSL OIM 6.0 analysis software to obtain the dislocation distribution.

The TEM specimens were ground into thin foils of 60−80 μm, and then a disc with a diameter of 3 mm was rushed out of the thin foils, and the thin foils were thinned by double spraying. The T4 and

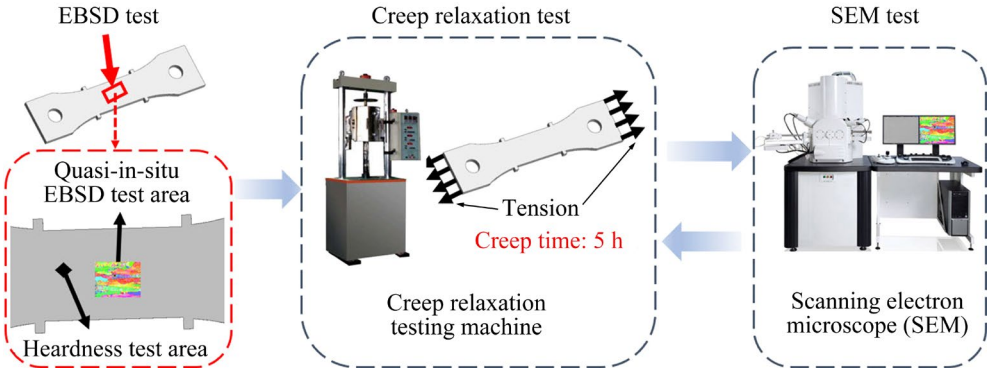

Fig. 3 Schematic diagrams of quasi-in-situ EBSD test

T6 specimens were electropolished at −25 °C and 16 V using the MTP−1 twinjet, and the electrolyte solution was taken with 30% HNO_3 + 70% CH_3OH (volume fraction) solution. The microstructure of the specimens was observed by the Talos F200X TEM, and bright-field scanning TEM and high-resolution TEM (HRTEM) images of the precipitates were obtained in the $[110]_{Al}$ direction. With Image J software for strengthening phase (GP I zone and η' phase) of average size information, the number of TEM images used for statistics in each heat treatment state is not less than three. A Digital Micrograph plug-in (DM 3.41.2916.1 package, HREM Research Inc.) was used for geometric phase analysis (GPA).

3 Results

3.1 Creep deformation behavior

Figure 4 presents the creep deformation behavior of specimens subjected to different heat treatments. The final creep strains of the T4 and T6 specimens were 0.52% and 0.45%, respectively (Fig. 4(a)). As shown in Fig. 4(b), after entering the second stage of creep, the creep rates of the T4 and T6 specimens tend to be stabilized at approximately 2.11×10^{-8} and 1.44×10^{-8} s^{-1}, respectively. Besides, it can be obviously seen that the creep curves are divided into two stages: the initial stage and the stable stage. It is noteworthy that the initial stage of the creep curve is relatively brief, lasting for approximately 0.5 h. However, the strain during this stage reaches more than 70% of the total creep strain, which is attributed to the increased dislocation diffusion rate due to the high strain rate.

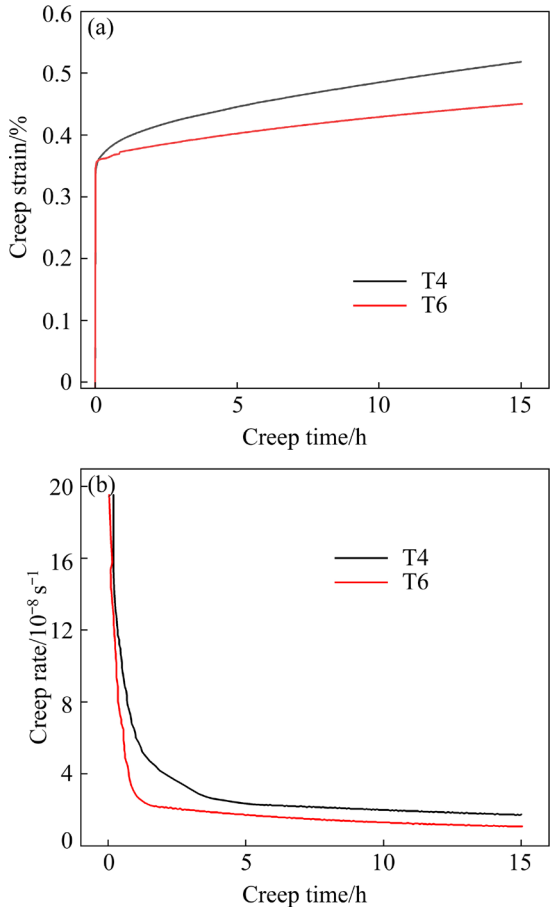

Fig. 4 Creep strain (a) and corresponding creep rate (b) curves of different specimens at 200 MPa and 150 °C

3.2 Quasi-in-situ EBSD analysis results for creep aging processes

Figures 5(a−d) and 6(a−d) illustrate the microstructure evolution of the T4 and T6 specimens during creep aging under initial heat treatment states. The analyzed cross section comprised the rolling direction (RD) and transverse direction (TD). It should be mentioned here that there is a slight displacement among these images since the scanning areas are manually aligned, but this does not significantly affect the results of the present study. It is obvious that the boundary structure and orientation distribution of the Al−Zn−Mg−Cu alloy have remained basically stable during creep aging. The average grain size of T4 and T6 specimens obtained by EBSD analysis software (Channel 5) is 107.6 and 154.1 μm, respectively.

Dislocation density variations play a crucial role in the thermal deformation process of metallic materials and provide insight into the active microstructural evolution mechanisms [28], the evolution of kernel average misorientation (KAM) during creep is discussed in this study.

Figures 5(e−h) and 6(e−h) show the KAM diagrams of Al−Zn−Mg−Cu alloy samples after T4 and T6 pre-heat treatments with varying levels of creep deformation. The misorientation for each deformation level ranges from 0° (Min) to 5° (Max), as indicated by the color band. The effect of low strain levels on dislocation proliferation is limited, though a gradual uniform distribution of dislocation can still be observed. With the creep aging of T4 and T6 specimens, the clear yellow line in the grain crystals thickens, while the internal color contrast diminishes. The KAM color gradient gradually shifts from blue to green and yellow, indicating that the strain region expands, and the internal storage energy

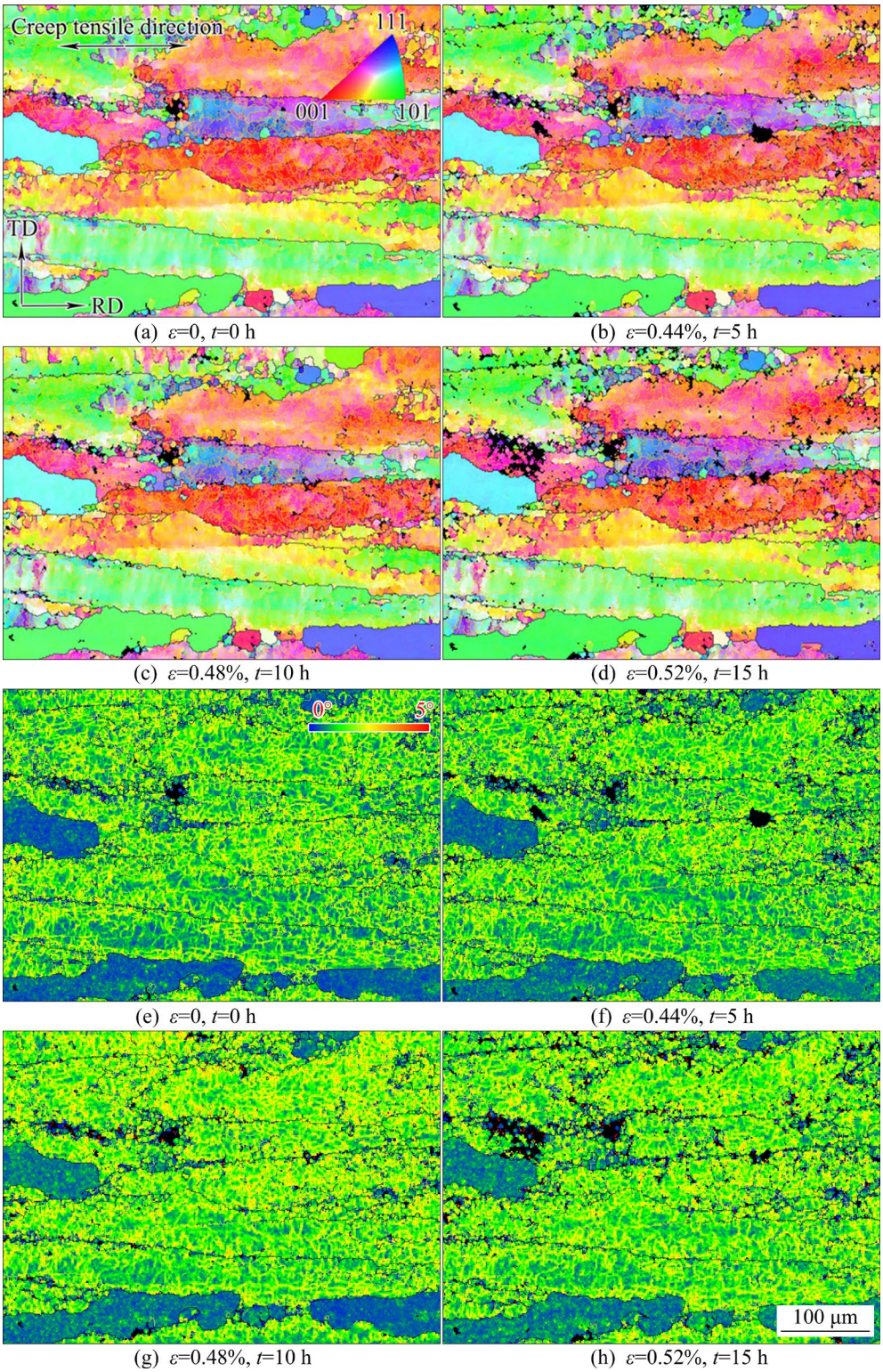

(a) ε=0, t=0 h (b) ε=0.44%, t=5 h

(c) ε=0.48%, t=10 h (d) ε=0.52%, t=15 h

(e) ε=0, t=0 h (f) ε=0.44%, t=5 h

(g) ε=0.48%, t=10 h (h) ε=0.52%, t=15 h

Fig. 5 Typical inverse pole figures (IPFs) (a−d) and corresponding KAM maps (e−h) of T4 specimen after creep tensile test at 150 °C: (a, e) T4; (b, f) T4+(CA, 5 h); (c, g) T4+(CA, 10 h); (d, h) T4+(CA, 15 h) (CA: Creep aging)

of the grains increases. This suggests that the disparity between regions of higher and lower dislocation density decreases during creep stretching, meaning the plastic deformation induced by creep becomes globally coordinated, and the dislocation distribution within the microstructure becomes increasingly uniform.

To evaluate the evolution of dislocation density in specimens subjected to various strains and aging time, the GND density (ρ_{GND}) was calculated from the

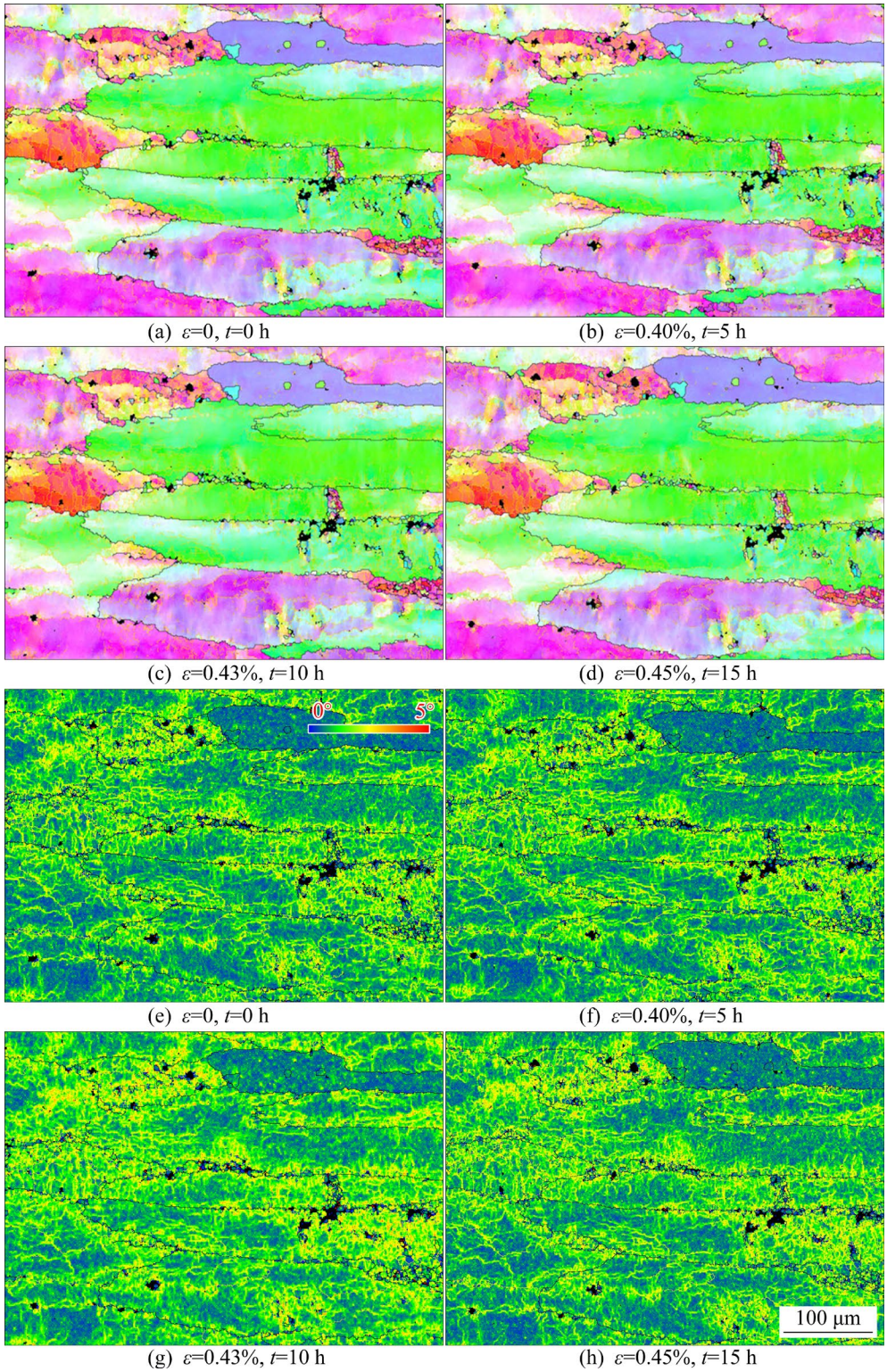

Fig. 6 Typical IPFs (a−d) and corresponding KAM maps (e−f) of T6 specimen after creep tensile test at 150 °C: (a, e) T6; (b, f) T6+(CA, 5 h); (c, g) T6+(CA, 10 h); (d, h) T6+(CA, 15 h)

kernel average misorientation (KAM) using standard EBSD data processing software packages [29]:

$$\rho_{\mathrm{GND}}=\alpha\frac{\mathrm{KAM}}{bR} \tag{1}$$

where α is a constant that depends on the nature of dislocation edge or screw, and a value α=3 was proposed [30]; KAM values are given by the EBSD software (TSL OIM 6.0); b is the magnitude of the Burgers vector (0.286 nm is used for Al); R is the kernel size taking into account the neighbor order

considered in the KAM map (R is 1.2 μm).

During the creep aging process, the dislocation density of specimens under different initial heat treatment conditions evolved differently. The evolution of GND density in T4 and T6 specimens is illustrated in Fig. 7. Moreover, the T4 specimen exhibits a significantly higher dislocation density compared to the T6 specimen. This is attributed to the dislocation recovery during aging as the diffusion of the atoms increases at high temperatures. As the energy supplied during the dislocation recovery process increases, the total number of dislocations correspondingly decreases [31,32].

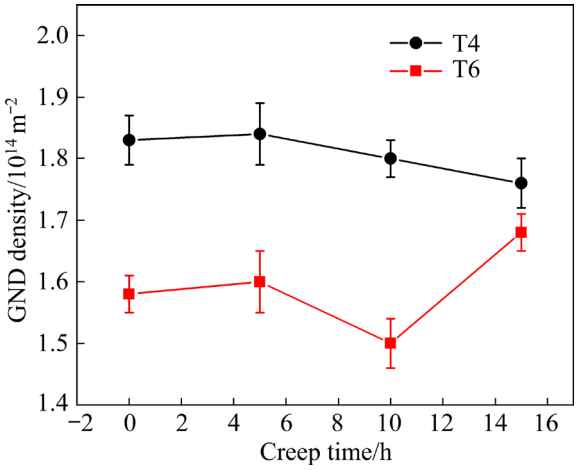

Fig. 7 GND density evolution of T4 and T6 specimens during creep aging

More than 80% of the total creep strain occurred within the first 5 h, which accounted for the increase in dislocation density observed during the initial stage of creep aging. The dislocation density of T4 and T6 specimens increased from 1.83×10^{14} and 1.58×10^{14} m^{-2} up to 1.84×10^{14} and 1.60×10^{14} m^{-2}, respectively as the creep time increased from 0 to 5 h. After entering the steady state stage of creep aging, a dynamic dislocation density evolution process occurred due to the multiplication and proliferation of dislocations. The GND density of the T6 specimen significantly increased from 10 to 15 h and was higher than that at 5 h. This phenomenon is attributed to the coarsening of precipitates during the creep aging of peak-aged samples, which hinders the movement of dislocations around the precipitates [33]. The dislocation pile-up rate near the coarse precipitated phase exceeds the annihilation rate of dislocation caused by aging heat treatment. Thus, it can be inferred that dislocation activity is one of the dominant mechanisms in creep deformation.

Figure 8 shows the grain boundary (GB) maps

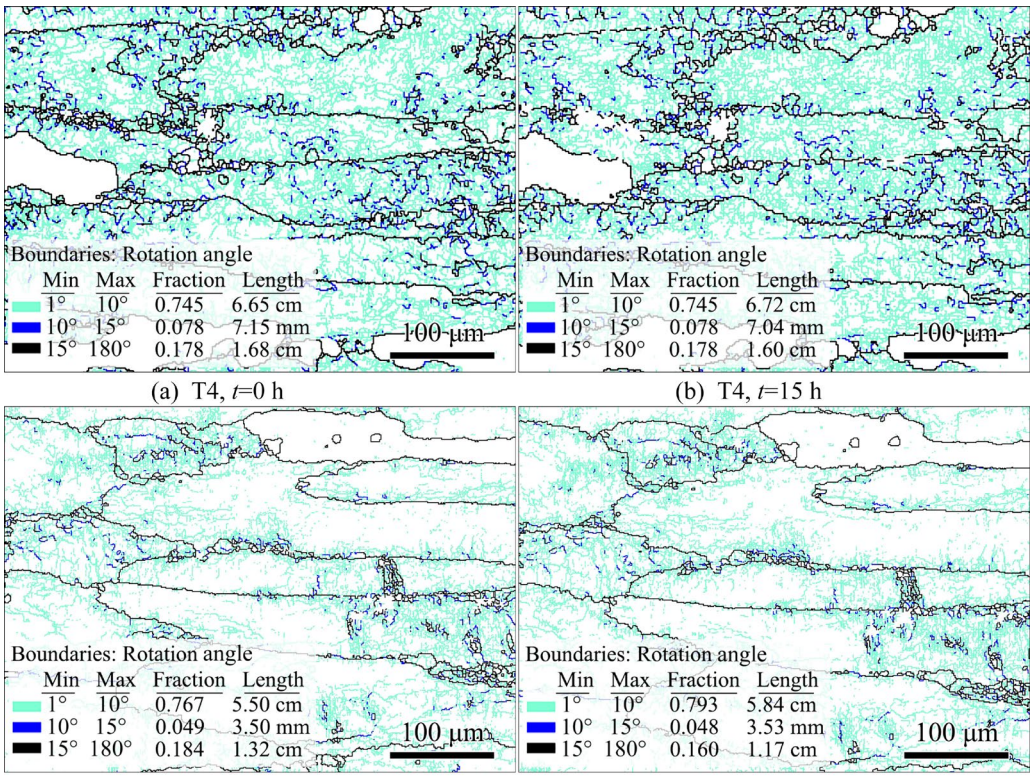

Fig. 8 GB maps of different specimens: (a) T4; (b) T4+(CA, 15 h); (c) T6; (d) T6+(CA, 15 h)

of T4 and T6 specimens before and after the creep aging process. Low-angle grain boundaries (LAGBs, 1°−10°), medium-angle grain boundaries (MAGBs, 10°−15°) and high-angle grain boundaries (HAGBs, >15°) are indicated by different colored lines. LAGBs, MAGBs and HAGBs are represented by cyan, blue and black lines, respectively. Notably, both T4 and T6 specimens exhibited a large proportion of LAGBs (~75%) in the grains before creep aging, with a slight increase observed after creep aging: 1.0% in the T4 specimen and 2.6% in the T6 specimen. This increase is attributed to the slip and climb of dislocations, which form substructures and consequently promote the development of LAGBs. For MAGBs, both specimens showed a slight decrease of 0.1%, remaining essentially unchanged. The main reduction was in the HAGBs, with a 0.8% decrease in the T4 specimen and a 1.68% decrease in the T6 specimen. Additionally, the thermal energy introduced during the creep aging process significantly enhanced the atomic diffusion within the material, thereby increasing dislocation mobility. The increased dislocation mobility led to subgrain rotation, which may occur through grain boundary sliding (GBS) [34] and absorption of dislocations into subgrain boundaries [35]. Consequently, the accumulation and movement of dislocations continuously form new subgrain boundaries. This observation aligns with the experimental results showing an increase in LAGBs and a decrease in HAGBs during creep aging.

3.3 Precipitation after aging treatment

The creep behavior and final mechanical properties of materials during creep aging largely depend on the initial precipitation state. Therefore, TEM tests were conducted to elucidate the underlying microscopic mechanisms. The precipitation path of Al−Zn−Mg−Cu alloy is: SSSS → GP zones → η' phase→ η phase [36,37].

From the TEM bright field images in Fig. 9, both T4 and T6 specimens have some dispersed particles with an average size of 30−50 nm in the Al matrix. There is no obvious precipitate in the Al matrix of T4 specimen, while the η' phase is mainly

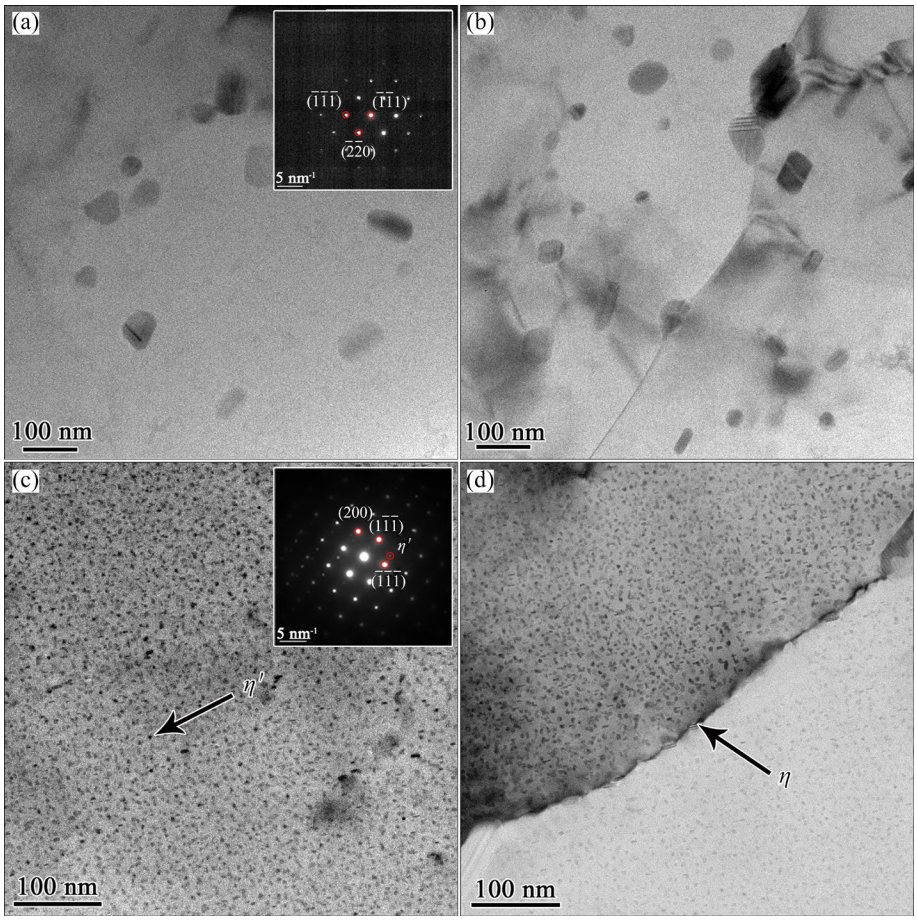

Fig. 9 TEM bright field images of Al−Zn−Mg−Cu alloy taken from intragranular regions and grain boundaries viewed along ⟨110⟩ zone axis: (a, b) T4 specimen; (c, d) T6 specimen

dispersed and evenly distributed in the Al matrix of T6 specimen. And the radius of the η' phase under T6 heat treatment is r_{T6}=(1.9±0.1) nm. The η phase with a size of 16.03 nm × 5.84 nm exists at the grain boundaries of the specimen in the peak aging state, and the mean distance is (20.51±4.32) nm.

Figure 10(a) shows the HRTEM image along the $[110]_{Al}$ direction. The Fast Fourier Transform (FFT) analysis indicates that the GP I zone is coherent with the Al matrix. Due to the presence of the coherent GP I zone, contrast differences are observed in the HRTEM image. The lattice distortion near the GP I zone can be visually observed by the strain field distribution, so the spherical GP I zone (marked by a white circle in the figure) can be easily labeled. The size of the strain field was measured using the Image J software and taken as the effective size of the GP zone. The radius of GP I zone in T4 specimen is (1.4±0.2) nm. Additionally, only GP I zone is formed in Al−Zn−Mg−Cu alloy which is naturally aged at room temperature after solution quenching treatment [38,39]. Figure 10(c) indicates

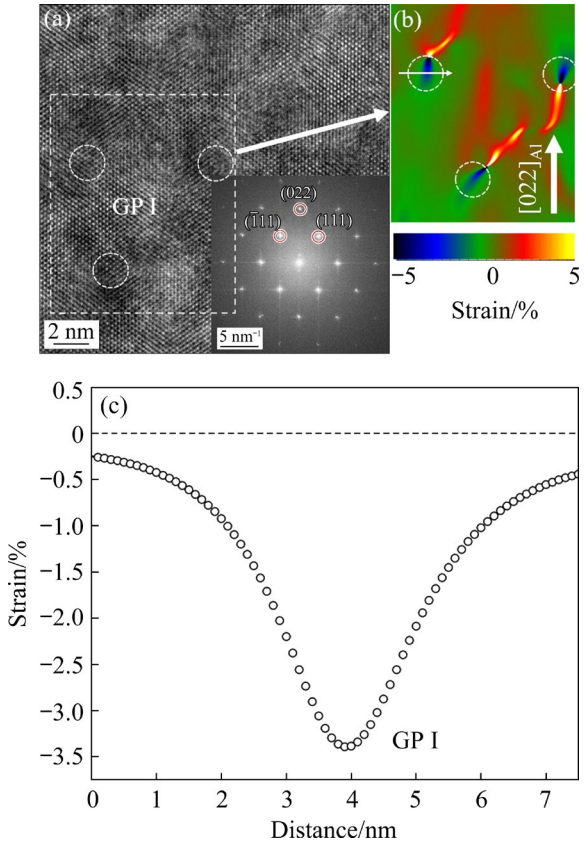

Fig. 10 (a) HRTEM image of GP I zone of T4 specimen and corresponding FFT (inserted at the lower right corner); (b) Strain field map in white dotted box in (a); (c) Linear strain distribution in GP I zone

that the strain along the (022) plane of the GP I zone is contracted by a value of up to ~3.2% for the Al lattice. The small GP I zone and strengthening precipitates η' (1−2 nm in size) play a crucial role in the creep properties of the alloy, as they can be cut through or bypassed by dislocations. The peak-aged alloy primarily contains η' phase, with its habit planes (facets) parallel to the $\{111\}_{Al}$ planes [40]. During plastic deformation, these hexagon disks of strengthening precipitates act as effective barriers to dislocation motion [41]. As shown in Table 1, the size of the unsteady GP I zone in the T4 specimen is smaller than that of the steady η' phase. The area fraction of the strengthening precipitates in the T4 specimen is 8.65%, which is less than 13.21% in the T6 specimen. Combined with the above creep behavior test results, the T4 specimen exhibits better creep formability. It can be inferred that the GP I zone in the T4 specimen has a weaker capacity to hinder the dislocation movement.

Table 1 Information of precipitates under different aging conditions

Aging condition	Precipitate	Radius/nm	Area fraction/%
25 °C, 168 h (T4)	GP I zone	1.4±0.4	8.65±3.41
120 °C, 24 h (T6)	η' phase	1.9±0.2	13.21±2.35

4 Discussion

4.1 Orientation dependence of creep aging of Al−Zn−Mg−Cu alloys

The Schmid factor (SF) can be used to measure the difficulty of grain deformation by dislocation slips in the current state. As shown in Fig. 11, the distribution of Schmid factor values is not uniform. The difficulty of dislocation slip is closely related to the rotations of orientation, which is called geometrical hardening/softening [42]. Grains with hard orientations (characterized by a low SF) present strong barriers to dislocation motion and slip system activation, thereby impeding plastic deformation within those grains. Based on existing research, the discussion will focus on two factors: SF and crystallographic orientation.

To reveal the effect of creep aging on substructure evolution and dislocation movement of aluminum matrix grains, typical grains were selected

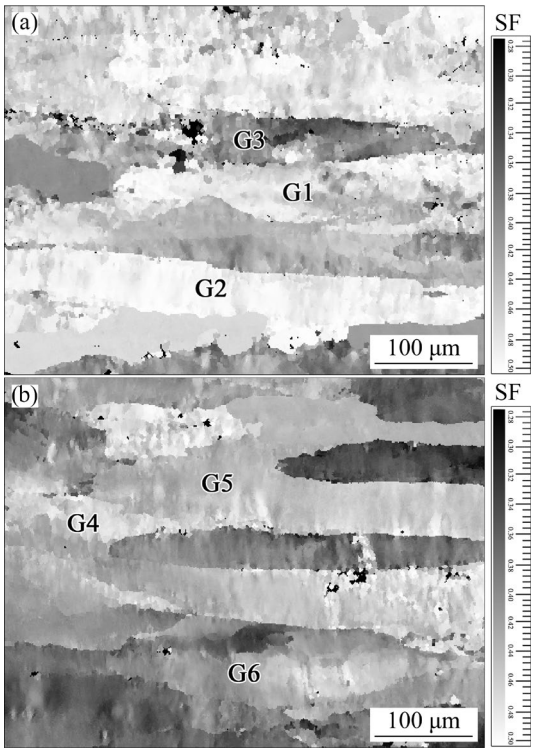

Fig. 11 Distribution of Schmid factors of different specimens: (a) T4 specimen; (b) T6 specimen

from the initial grains of T4 and T6 specimens and as numbered G1−G6. G1 and G4 are close to ⟨001⟩ orientation, G2 and G5 are close to ⟨101⟩ orientation, and G3 and G6 are close to ⟨111⟩ orientation.

Figure 12 shows misorientation profiles of typical grains along RD during creep aging in T4 and T6 specimens after different routes and passes. The solid black line in Fig. 12 represents the point-to-point misorientations in different initial heat treatment states along the RD direction, while the red, blue, and green lines correspond to the misorientations along the RD direction after 5, 10, and 15 h of creep, respectively. The orientation deviation gradually increases with the increase of strain during creep aging, indicating more pronounced grain rotation. For specimens with different heat treatment states, the orientation deviation before and after creep gradually increases and decreases at the subgrain boundaries, respectively. The larger the initial orientation deviation (marked by the red dotted box in the figure), the more significant the change in the orientation deviation value after creep aging. The region with smaller initial orientation deviation (marked by the blue dotted line box in the figure) is more stable during creep aging.

The maximum orientation deviations of G1 and G4 with high SF soft orientation are 7° and 6°, respectively, for G2 and G5 they are 7° and 5°, respectively, and for G3 and G6 with low SF hard orientations, the deviations are 5° and 2°, respectively. The orientation gradients of G1, G2 and G4 in soft orientation grains surrounded by hard orientation grains, vary more significantly compared to other grains in this investigation.

The results indicate that dislocation movement is primarily concentrated at the subgrain boundaries, and grains with soft orientations and high SF provide less resistance to dislocation movement during the creep aging process. Additionally, the grain orientation deviation near the ⟨001⟩ and ⟨101⟩ orientations exhibits the most significant changes. In general, the orientation deviation in T4 specimen after creep aging is greater than that in T6 specimen, which may be attributed to the varying resistance to dislocation movement due to different degrees of precipitation.

4.2 Strengthening contribution of GP I zones and η' precipitates

For creep-age forming, the strengthening mechanism of Al−Zn−Mg−Cu alloy is mainly solid solution strengthening (σ_{ss}), grain boundary strengthening (σ_{gb}), dislocation strengthening (σ_d), and precipitation strengthening (σ_p) can be calculated by the following equation [5,43,44]:

$$\sigma_y=\sigma_o+\sigma_{ss}+\sigma_{gb}+\sigma_d+\sigma_p \quad (2)$$

where σ_y is the yield strength of specimens. σ_o (=35 MPa) is the yield strength of Al matrix [45]. σ_{ss} can be expressed as [46]

$$\sigma_{ss}=\sum_j h_j c_j^{2/3} \quad (3)$$

where h_j represents the parameter of alloying element j. The values of h for Zn, Mg and Cu elements are 2.9, 18.6 and 13.6 MPa/(wt.%)$^{2/3}$, respectively. c is the alloy element concentration. By substituting h value into Eq. (3), the solid solution strengthening value is 52.5 MPa.

Grain boundary strengthening (σ_{gb}) is generally described by the Hall−Petch equation [47]:

$$\sigma_{gb}=kd^{-1/2} \quad (4)$$

where k is the Hall−Petch slope, and set as 0.14 MPa·m$^{-1/2}$ in this study [48]. Previous EBSD test results showed that creep aging treatment did not

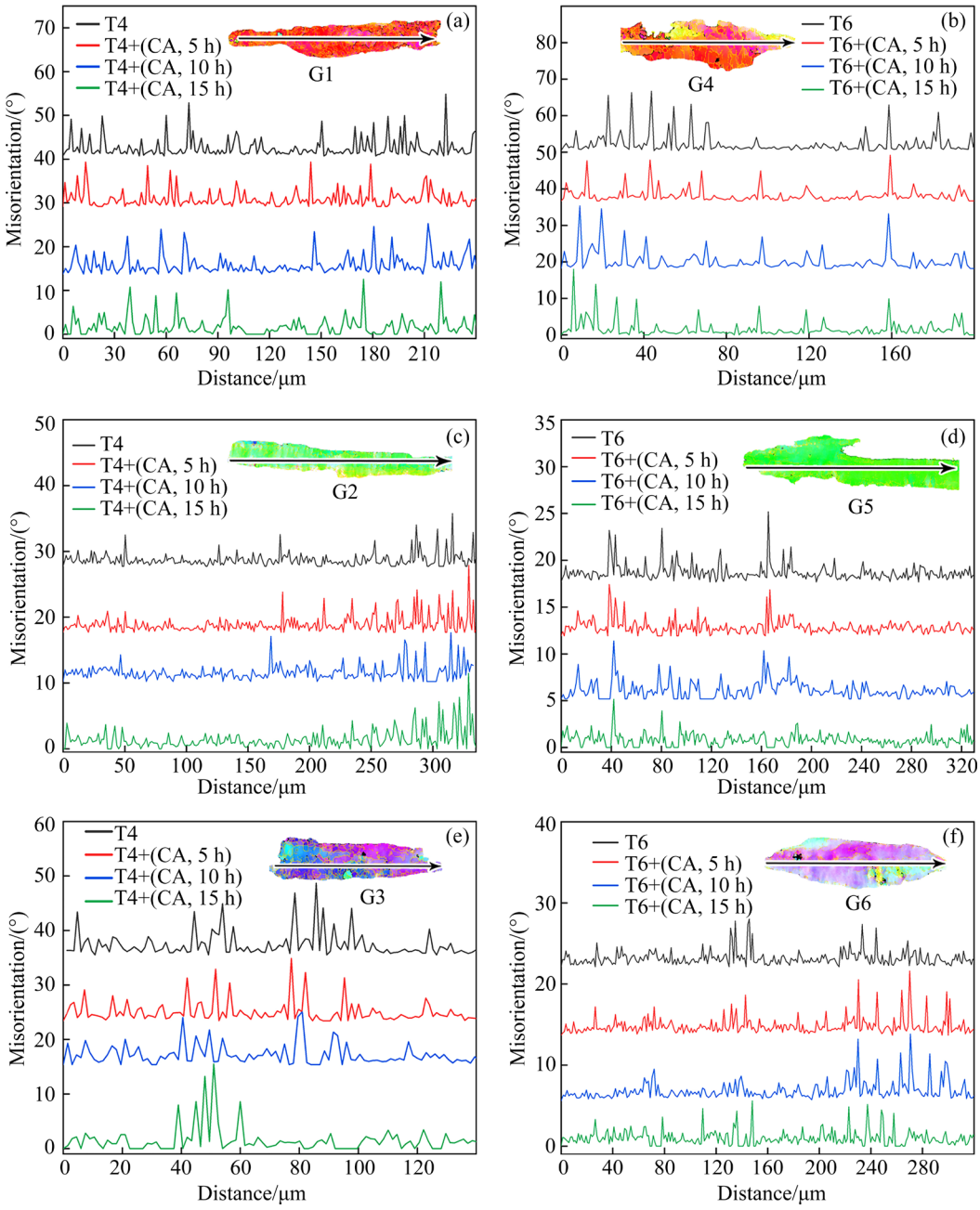

Fig. 12 Misorientation profiles of typical grains along RD during creep aging in T4 and T6 specimens after different routes and passes: (a, b) ⟨001⟩ orientation; (c, d) ⟨101⟩ orientation; (e, f) ⟨111⟩ orientation

cause changes in grain shape. Substituting the average grain size (d) into Eq. (4), it can be seen that the grain boundary strengthening (σ_{gb}) values of T4 and T6 specimens are 13.5 and 11.3 MPa, respectively [29].

Dislocation strengthening (σ_d) can be calculated using the Bailey−Hirsch equation [29]:

$$\sigma_d=M\alpha Gb\rho^{1/2} \quad (5)$$

where M is the mean orientation factor (3.06 for fcc metals), α is a constant (0.2 for fcc metals), G=(26.9 GPa) is the shear modulus of Al matrix, and ρ is the dislocation density consisting of geometrically necessary dislocations (ρ_{GND}) and statistically stored dislocations (ρ_{SSD}). Creep deformation is generally considered as a small deformation (generally creep strain ε<2%), in which GNDs play a leading role [49], so the value of ρ is directly taken as ρ_{GND} in this study. Substituting the ρ_{GND} into Eq. (5), it can be seen that the dislocation strengthening (σ_d) values of T4 and T6 specimens are 63.7 and 59.2 MPa, respectively.

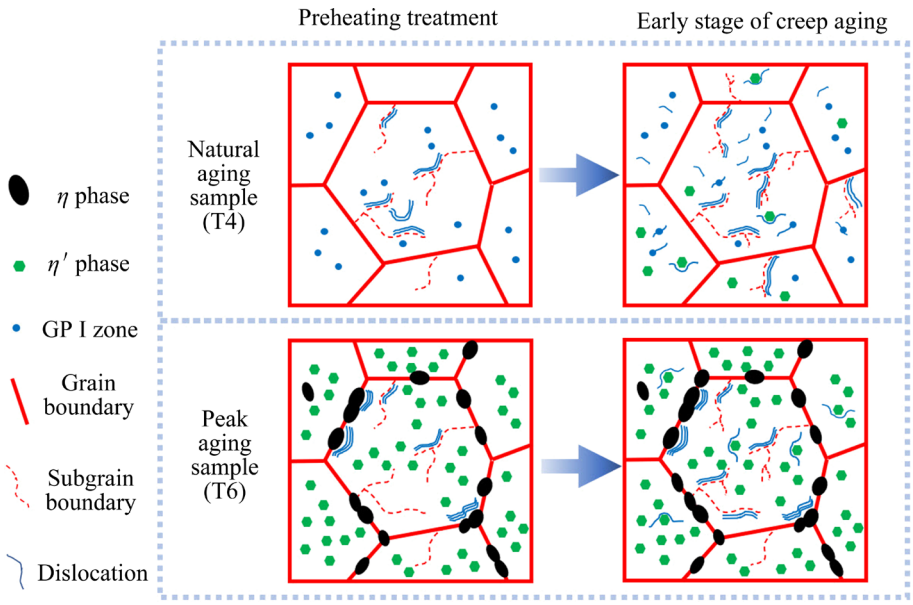

Fig. 13 Schematic diagrams of microstructure evolution of Al−Zn−Mg−Cu alloy treated by T4 and T6 pre-aging to early stage of creep aging

The precipitation strengthening effect of Al−Zn−Mg−Cu alloy under natural aging treatment (T4) is primarily attributed to the GP I zone. In contrast, after peak aging treatment (T6), a high-density dispersed η' phase is formed in the Al matrix, becoming the primary source of resistance to dislocation movement. The mechanism of precipitation strengthening under these two heat treatment conditions is complicated, and σ_p can be estimated by Eq. (2).

The yield strength σ_y of T4 and T6 specimens obtained by tensile test at room temperature is 310.0 and 495.5 MPa, respectively. Using Eqs. (2)−(5), the precipitation strengthening (σ_p) values for T4 and T6 heat treatment conditions were calculated to be 145.3 and 337.5 MPa, respectively. This suggests that the high density dispersed η' phase can provide higher resistance to the dislocation movement, which is consistent with the results of the uniaxial creep tensile test ($\varepsilon_{T4}>\varepsilon_{T6}$).

Considering that the first stage creep strain accounts for more than 70% of the total creep strain, the evolution of dislocation and precipitation enters a dynamic stage during subsequent creep aging process. Figure 13 illustrates the microstructure evolution of Al−Zn−Mg−Cu alloy from natural aging and peak aging treatment to the early stage of creep aging. After rolling and solution-aging treatment, there is a high proportion of subgrain boundaries in the initial grain of the specimens, and the dislocations are mainly distributed at the grain boundaries and subgrain boundaries. In the T4 specimens, the GP I zones are mainly dispersed, whereas in the T6 specimens, the η' phase is densely and uniformly distributed within the Al matrix, with continuous η phase observed along the grain boundaries. The GND density of T6 specimen is lower than that of T4 specimen.

After entering the first stage of creep aging, the GND density in both specimens increases as creep strain increases. Dislocations propagate along grain and subgrain boundaries, becoming entangled to form dislocation cells and high-density dislocation regions, which further increase the proportion of subgrains. Simultaneously, the complex interactions among the GP I zone, fine η' phase, stable η phase, and dislocations alter the dislocation propagation path, leading to a more uniform distribution of dislocations in the Al matrix.

5 Conclusions

(1) The creep formability of T4 specimens is better than that of T6 specimens. The creep strain of Al−Zn−Mg−Cu alloy at 200 MPa and 150 °C for 15 h is ordered as: ε_{T4} (0.52%) > ε_{T6} (0.45%).

(2) The density of geometrically necessary dislocations increases during the initial creep stage

(<0.5 h) and undergoes dynamic changes during the stable creep stage. Creep aging treatment can effectively improve the dislocation distribution inhomogeneity within the Al−Zn−Mg−Cu alloy, leading to an increase in LAGBs and a decrease in HAGBs during the creep aging process.

(3) Creep aging of Al−Zn−Mg−Cu alloy exhibits preferential deformation orientations. Quasi-in-situ EBSD analysis reveals that the grain orientations more prone to dislocation movement are ⟨001⟩ and ⟨101⟩ orientations, both of which are soft orientations (high Schmid factor) that are prone to deformation during the creep process.

(4) Different creep deformations in pre-aged Al−Zn−Mg−Cu alloys indicate that the pre-existing precipitates and dislocations fundamentally alter the microstructure evolution during creep aging. Based on the strength model, the inhibitory effects of η' phase in T6 specimen and GP I zone in T4 specimen on dislocation movement were considered. The creep formability and post-forming properties of Al−Zn−Mg−Cu alloys can be jointly improved by reducing the initial precipitation degree.

CRediT authorship contribution statement

Chuan GAO: Investigation, Methodology, Writing − Original draft preparation; **Xiao-bin GUO:** Methodology, Supervision, Methodology, Formal analysis; **Feng-quan WANG:** Data curation; **Chao-jie LIANG:** Writing – Review & editing; **Yun-lai DENG:** Supervision, Conceptualization, Funding acquisition, Project administration.

Declaration of competing interest

The authors declare that they have no known competing financial interests or personal relationships that could have appeared to influence the work reported in this paper.

Acknowledgments

The authors gratefully acknowledge the support from the National Key Research and Development Program of China (No. 2023YFB3710501).

References

[1] WILLIAMS J C, STARKE E A. Progress in structural materials for aerospace systems [J]. Acta Materialia, 2003, 51: 5775−5799.

[2] JEUNECHAMPS P P, HO K C, LIN J, PONTHOT J P, DEAN T A. A closed form technique to predict springback in creep age-forming [J]. International Journal of Mechanical Sciences, 2006, 48: 621−629.

[3] FAN Cai-he, LI Yi-hui, WU Qin, OU Ling, HU Ze-yi, NI Yu-meng, YANG Jian-jun. Effect of cold rolling deformation on microstructure evolution and mechanical properties of spray formed Al−Zn−Mg−Cu−Cr alloys [J]. Transactions of Nonferrous Metals Society of China, 2024, 34: 2442−2454.

[4] ZHANG Zhen, DENG Yun-lai, YE Lin-ying, ZHU Wen-bo, WANG Feng-quan, JIANG Ke-da, GUO Xiao-bin. Influence of aging treatments on the strength and localized corrosion resistance of aged Al−Zn−Mg−Cu alloy [J]. Journal of Alloys and Compounds, 2020, 846: 156223.

[5] WEI Peng-fei, HU Zhi-li, PANG Qiu. Microstructure evolution and strengthening mechanisms of high strength Al−Zn−Mg−Cu alloy via pre-hardening forming [J]. Journal of Alloys and Compounds, 2023, 968: 172057.

[6] WANG Yi-chang, WU Xiao-dong, YUE Lu, GUO Ming-xing, CAO Ling-fei. Aging precipitation behavior and properties of Al−Zn−Mg−Cu−Zr−Er alloy at different quenching rates [J]. Transactions of Nonferrous Metals Society of China, 2022, 32: 1070−1082.

[7] ZHENG Jing-hua, PAN Ran, LI Chen, ZHANG Wei, LIN Jiang-guo, DAVIES C M. Experimental investigation of multi-step stress-relaxation-ageing of 7050 aluminium alloy for different pre-strained conditions [J]. Materials Science and Engineering: A, 2018, 710: 111−120.

[8] WANG D, NI D R, MA Z Y. Effect of pre-strain and two-step aging on microstructure and stress corrosion cracking of 7050 alloy [J]. Materials Science and Engineering: A, 2008, 494: 360−366.

[9] YANG Wen-chao, JI Shou-xun, ZHANG Qian, WANG Ming-pu. Investigation of mechanical and corrosion properties of an Al−Zn−Mg−Cu alloy under various ageing conditions and interface analysis of η' precipitate [J]. Materials & Design, 2015, 85: 752−761.

[10] ZOU Yan, WU Xiao-dong, TANG Song-bai, ZHAO Kai, CAO Ling-fei. Tailoring phase fractions of T' and η' phases in dual-phase strengthened Al−Zn−Mg−Cu alloy via ageing treatment [J]. Transactions of Nonferrous Metals Society of China, 2022, 32: 3182−3196.

[11] HOLMAN M C. Autoclave age forming large aluminum aircraft panels [J]. Journal of Mechanical Working Technology, 1989, 20: 477−488.

[12] JESHVAGHANI R A, SHAHVERDI H R, HADAVI S M M. Investigation of the age hardening and operative deformation mechanism of 7075 aluminum alloy under creep forming [J]. Materials Science and Engineering: A, 2012, 552: 172−178.

[13] HAN Nian-mei, ZHANG Xin-ming, LIU Sheng-dan, KE Bin, XIN Xing. Effects of pre-stretching and ageing on the strength and fracture toughness of aluminum alloy 7050 [J]. Materials Science and Engineering: A, 2011, 528: 3714−3721.

[14] GAO Han-jun, WU Shao-feng, WU Qiong, LI Bian-hong, GAO Zi-han, ZHANG Yi-du, MO Shuai. Experimental and simulation investigation on thermal-vibratory stress relief process for 7075 aluminium alloy [J]. Materials & Design, 2020, 195: 108954.

[15] XU Ling-zhi, TONG Can-yu, ZHAN Li-hua, XU Yong-qian, LIU Chun-hui, HUANG Ming-hui, YANG You-liang, MA

Bo-lin, WANG Yong-mei. Improved creep forming efficiency and retained performance via a novel two-stage creep aging process of Al−Zn−Mg−Cu alloys [J]. Materials Science and Engineering: A, 2022, 851: 143581.

[16] LIN Yong-cheng, ZHANG Jin-long, LIU Guan, LIANG Ying-jie. Effects of pre-treatments on aging precipitates and corrosion resistance of a creep-aged Al−Zn−Mg−Cu alloy [J]. Materials & Design, 2015, 83: 866−875.

[17] MA Zi-yao, LIU Chun-hui, XU Ling-zhi, HUANG Ming-hui, YANG You-liang, XU Yong-qian, MA Bo-lin, ZHAN Li-hua. Pre-strain-dependent creep ageing behavior of an Al−Cu alloy [J]. Materials Characterization, 2022, 192: 112225.

[18] DAI Hao-fang, XU Guo-fu, LI Yao, GUO Guang-yi, PENG Xiao-yan. Effects of electropulsing frequency on mechanical properties, corrosion behavior and microstructure of a creep-aged 7050 aluminum alloy [J]. Materials Characterization, 2022, 194: 112386.

[19] MAHATHANINWONG N, ZHOU Y, BABCOCK S E, PLOOKPHOL T, WANNASIN J, WISUTMETHANGOON S. Creep rupture behavior of semi-solid cast 7075-T6 Al alloy [J]. Materials Science and Engineering: A, 2012, 556: 107−113.

[20] WANG Xiang-dong, PAN Qing-lin, WANG Wei-yi, HUANG Zhi-qi, CHEN Jian, PAN Bai-qing, LIU Xiong. Effects of pre-strain and aging treatments on the mechanical property and corrosion resistance of the spray formed ultra-high strength Al−Zn−Mg−Cu alloy [J]. Materials Characterization, 2022, 194: 112381.

[21] LU Jue, SONG Yan-li, HUA Lin, ZHENG Kai-lun, DAI Ding-guo. Thermal deformation behavior and processing maps of 7075 aluminum alloy sheet based on isothermal uniaxial tensile tests [J]. Journal of Alloys and Compounds, 2018, 767: 856−869.

[22] GAO Yin-jun, HUANG Zong-jin, DENG Qian-qian, LIAO Kun, LI Yi-xuan, YI Xiao-yi, LUO Zhi-rong. Structural transformation and energy analysis for pile-up dislocations at triple junction of grain boundary [J]. Transactions of Nonferrous Metals Society of China, 2022, 32: 45−63.

[23] LU Jue, SONG Yan-li, ZHOU Pu, XU Hai-nan, LIU Yu-jian, HUA Lin. Effect of thermal strain on the microstructure evolution and post-aging mechanical properties of Al−Zn−Mg−Cu alloy in simulating hot stamping process [J]. Materials Science and Engineering: A, 2023, 880: 145316.

[24] WANG Xi, RONG Qi, SHI Zhu-sheng, LI Yong, CAO Jun-xia, CHEN Bao-guo, LIN Jiang-guo. Investigation of stress effect on creep, precipitation and dislocation evolution of Al−Li alloy during creep age forming [J]. Materials Science and Engineering: A, 2022, 836: 142723.

[25] GAO Chuan, DENG Yun-lai, WANG Feng-quan, GUO Xiao-bin. Effect of creep aging on mechanical properties of under-aged 7075 aluminum alloy [J]. Acta Metallurgica Sinica, 2022, 58: 746−759. (in Chinese)

[26] ABACHI P, PURAZRANG K. The correlation between fracture mechanics parameters and creep crack growth rate of Al 7050-T73651 at elevated temperature [J]. Engineering Fracture Mechanics, 2015, 142: 276−286.

[27] HO K C, LIN J, DEAN T A. Constitutive modelling of primary creep for age forming an aluminium alloy [J]. Journal of Materials Processing Technology, 2004, 153/154: 122−127.

[28] NOLZE G, JÜRGENS M, OLBRICHT J, WINKELMANN A. Improving the precision of orientation measurements from technical materials via EBSD pattern matching [J]. Acta Materialia, 2018, 159: 408−415.

[29] ZRIBI Z, KTARI H H, HERBST F, OPTASANU V, NJAH N. EBSD, XRD and SRS characterization of a casting Al−7wt.%Si alloy processed by equal channel angular extrusion: Dislocation density evaluation [J]. Materials Characterization, 2019, 153: 190−198.

[30] KONIJNENBERG P J, ZAEFFERER S, RAABE D. Assessment of geometrically necessary dislocation levels derived by 3D EBSD [J]. Acta Materialia, 2015, 99: 402−414.

[31] HASS M D, HOSSON J T M D. Grain boundary segregation and precipitation in aluminium alloys [J]. Scripta Materialia, 2001, 44: 281−286.

[32] LIU Jin, DU Zhi-yong, SU Jin-long, TANG Jie, JIANG Fu-lin, FU Ding-fa, TENG Jie, ZHANG Hui. Effect of quenching residual stress on precipitation behaviour of 7085 aluminium alloy [J]. Journal of Materials Science & Technology, 2023, 132: 154−165.

[33] WANG Y, ZHAO H, CHEN X, GAULT B, BRECHET Y, HUTCHINSON C. The effect of shearable clusters and precipitates on dynamic recovery of Al alloys [J]. Acta Materialia, 2024, 265: 119643.

[34] YANG Xu-yue, MIURA H, SAKAI T. Continuous dynamic recrystallization in a superplastic 7075 aluminum alloy [J]. Materials Transactions, 2002, 43: 2400−2407.

[35] SUN Z C, WU H L, CAO J, YIN Z K. Modeling of continuous dynamic recrystallization of Al−Zn−Cu−Mg alloy during hot deformation based on the internal-state-variable (ISV) method [J]. International Journal of Plasticity, 2018, 106: 73−87.

[36] SHA G, CEREZO A. Early-stage precipitation in Al−Zn−Mg−Cu alloy (7050) [J]. Acta Materialia, 2004, 52: 4503−4516.

[37] ADRIEN J, MAIRE E, ESTEVEZ R, EHRSTROM J C, WARNER T. Influence of the thermomechanical treatment on the microplastic behaviour of a wrought Al−Zn−Mg−Cu alloy [J]. Acta Materialia, 2004, 52: 1653−1661.

[38] ZOU Yan, CAO Ling-fei, WU Xiao-dong, WANG Yi-chang, SUN Xu-an, SONG Hui, COUPER M J. Effect of ageing temperature on microstructure, mechanical property and corrosion behavior of aluminum alloy 7085 [J]. Journal of Alloys and Compounds, 2020, 823: 153792.

[39] LIU Sheng-dan, ZHANG Meng-han, LI Qun, ZHU Qian-qian, SONG Hui, WU Xiao-dong, CAO Ling-fei, COUPER M J. Effect of quenching rate on strengthening behavior of an Al−Zn−Mg−Cu alloy during natural ageing [J]. Materials Science and Engineering: A, 2020, 793: 139900.

[40] LIU Dong-mei, XIONG Bai-xiong, BIAN Feng-gang, LI Zhi-hui, LI Xi-wu, ZHANG Yon-gan, WANG Qiang-song, XIE Guo-liang, WANG Feng, LIU Hong-wei. Quantitative study of nanoscale precipitates in Al−Zn−Mg−Cu alloys with different chemical compositions [J]. Materials Science and Engineering: A, 2015, 639: 245−251.

[41] ROMETSCH P A, ZHANG Y, KNIGHT S. Heat treatment of 7xxx series aluminium alloys: Some recent developments [J]. Transactions of Nonferrous Metals Society of China, 2014, 24: 2003−2017.

[42] ASARO R J. Geometrical effects in the inhomogeneous deformation of ductile single crystals [J]. Acta Metallurgica,

1979, 27: 445−453.
[43] SUN Peng, HUANG Yu-sheng, SUN Lin-lin, LI Ya, ZHENG Xiao-yu, LI Bo, LI Xi-wu, YAN Hong-wei, LIU Yu-ling, DU Yong. Effect of heat treatment on microstructure evolution, strengthening mechanisms and mechanical properties of Zn modified Al−Mg alloys with Sc and Zr additions [J]. Materials Science and Engineering: A, 2024, 896: 146206.
[44] STARINK M J, WANG S C. A model for the yield strength of overaged Al−Zn−Mg−Cu alloys [J]. Acta Materialia, 2003, 51: 5131−5150.
[45] FAN Xiao-yu, LI Yu, XU Chun, WANG Bin-jun, PENG Rui-zhi, CHEN Jian-bin. Improved mechanical anisotropy and texture optimization of a 3xxx aluminum alloy by differential temperature rolling [J]. Materials Science and Engineering: A, 2021, 799: 140278.
[46] RYEN Ø, HOLMEDAL B, NIJS O, NES E, SJÖLANDER E, EKSTRÖM H. Strengthening mechanisms in solid solution aluminum alloys [J]. Metallurgical and Materials Transactions A, 2006, 37: 1999−2006.
[47] MA K K, WEN H M, HU T, TOPPING T D, ISHEIM D, SEIDMAN D N, LAVERNIA E J, SCHOENUNG J M. Mechanical behavior and strengthening mechanisms in ultrafine grain precipitation-strengthened aluminum alloy [J]. Acta Materialia, 2014, 62: 141−155.
[48] LLOYD D J, COURT S A. Influence of grain size on tensile properties of Al−Mg alloys [J]. Materials Science and Technology, 2003, 19: 1349−1354.
[49] WANG Nan, CHEN Yong-nan, WU Gang, ZHAO Qin-yang, ZHANG Zhen, ZHU Li-xia, LUO Jin-heng. Non-equivalence contribution of geometrically necessary dislocation and statistically stored dislocation in work-hardened metals [J]. Materials Science and Engineering: A, 2022, 836: 142728.

经不同时效处理 Al−Zn−Mg−Cu 合金在蠕变时效过程中的显微组织演变机理及蠕变响应

高 川[1]，郭晓斌[2]，王冯权[1]，梁朝杰[2]，邓运来[1,2]

1. 中南大学 轻合金研究院，长沙 410083；
2. 中南大学 材料科学与工程学院，长沙 410083

摘 要：研究了 Al−Zn−Mg−Cu 合金在不同初始热处理状态下的蠕变响应、力学性能和显微组织演变。结果表明：几何必要位错(GNDs)密度在初始蠕变阶段(<0.5 h)增大，在稳定蠕变阶段呈动态变化；随着蠕变时效的进行，晶内的位错分布逐渐均匀，形成了更多的亚晶。蠕变行为的主要影响因素是晶体取向和初始析出程度。取向为⟨001⟩和⟨101⟩的晶粒在蠕变过程中易发生变形。基于强度模型，评估了 T6 试样中 η'相和 T4 试样中 GP I 区对位错运动的抑制作用。研究表明，选择适当的初始析出状态是提高蠕变时效响应和获得高性能构件的有效策略。

关键词：Al−Zn−Mg−Cu 合金；蠕变时效；准原位 EBSD；显微组织；晶体取向；初始析出状态

(Edited by Wei-ping CHEN)